First experimental characterization of CaCl2 coated heat exchanger for thermochemical heat transformer applications in industrial waste heat recovery

Benoit Michel, Nicolas Dufour, Clémentine Börtlein, Camille Zoude, Elodie Prud'Homme, Laurent Gremillard, Marc Clausse

First experimental characterization of $CaCl_2$ coated heat exchanger for thermochemical heat transformer applications in industrial waste heat recovery

Benoit Michel[1*], Nicolas Dufour[1], Clémentine Börtlein[1], Camille Zoude[2], Elodie Prud'homme[2], Laurent Gremillard[2], Marc Clausse[1]

[1] *Univ Lyon, INSA Lyon, CNRS, CETHIL, UMR5008, 69621 Villeurbanne, France*
[2] *Univ Lyon, INSA Lyon, CNRS, MATEIS, UMR5510, 69621 Villeurbanne, France*
[*] *corresponding authors: benoit.michel@insa-lyon.fr*

Keywords:
Thermochemical Heat Transformer, Waste Heat, Salt coated heat exchanger

NOMENCLATURE

F_m	driving force *(-)*	*Subscripts*	
G	Reactive gas	eq	solid/gas equilibrium
M	molar weight ($kg{\cdot}mol^{-1}$)	E/C	evaporator/condenser
m	mass (*kg)*	htf	heat transfer fluid
p	pressure *(Pa)*	H	high temperature
$\dot{q}_m$	specific power ($W{\cdot}kg^{-1}$)	HX	heat exchanger
$\dot{Q}$	heat power (*W)*	i	inlet
Q	heat *(J)*	L	low temperature
R	ideal gas constant ($J{\cdot}mol^{-1}{\cdot}K^{-1}$)	m	medium (waste heat) temperature
S	reactive solid	max	maximum
T	temperature *(K or °C)*	v	vapor
X	reaction advancement ($mol_v.mol_s^{-1}$)	R	reactor
Greek symbols		s	salt
Δg_r	free Gibbs energy ($J{\cdot}mol^{-1}{}_s$)	0	dehydrated salt
Δh_r^0	standard enthalpy of reaction ($J{\cdot}mol^{-1}{}_v$)		
Δs_r^0	standard entropy of reaction ($J{\cdot}mol^{-1}{}_v{\cdot}K^{-1}$)	*Exponents*	
ν	stoichiometric coefficient ($mol_v.mol_s^{-1}$)	0	reference

Abstract

This study aims at evaluating the performance of a heat exchanger coated with $CaCl_2$ (PVA polyvinyl alcohol used as binder) for Thermochemical Heat Transformers (THT) applications in industrial waste heat recovery.

For this purpose, an experimental test bench has been built allowing to test operating temperatures up to 160 °C. A model heat exchanger plate is used to test two configurations: a thick layer of $CaCl_2$ to model a packed bed reactor (used as reference) and a $CaCl_2$-PVA deposit to model a coated reactor.

For the packed bed configuration, results comparable to that of the literature are obtained with a specific power of 180 W/kg obtained for a temperature lift of 60 K. A high sensitivity to temperature lift is identified with a decrease of the specific power down to 38 W/kg for a lift of 77 K. The coated heat exchanger configuration achieves significantly higher performance with a specific power up to 341 W/kg for a temperature lift of 63 K. However, the analysis of the repeatability tests highlights a rapid change in temperature profiles highlighting a change in properties of the $CaCl_2$/PVA compound material. Next steps will consist in enhanced material formulation and change in deposit protocol and to move to work at small reactor scale to assess system performance.

1. Introduction

Upgrading waste heat to higher temperatures is a lever to dramatically increase the energy efficiency of the industrial sector. In this sector which is a major energy consumer, the worldwide heat losses below 100 °C represent 3 722 TWh/year [1]. Thus, there is a great potential for reducing costs and increasing efficiencies in this sector. However, two main drawbacks are identified to valorize the available waste heat: the temperature level is too low to satisfy directly process requirements and the phase shift to the heat demand. To overcome these issues, several technologies such as heat storage and heat to heat conversion systems (heat pumps and heat transformers) have been studied in recent years [2–4].

Electrical Heat Pumps (EHP) have shown promising results in industrial heat recovery applications, but they still suffer from various drawbacks: excessive electricity consumption, low temperature lift, limited high temperature (most of EHP available on market can only achieve 130 °C as operating temperature), the lack of available refrigerants in the high temperature range with low GWP (Global Warming Potential) [4]. Additionally, process integration may require to store heat to handle variations in supply or demand, which in only achievable by adding a dedicated heat storage system while sorption heat transformer can deliver heat storage service to the process without adding an additional component [5].

Hence, sorption heat transformers, which use the heat generated by reversible absorption (liquid/gas), adsorption (solid/gas) or chemical (solid/gas) reactions, could be a good alternative to electrical heat pumps (EHP) in some cases.

Absorption Heat Transformers (AbHTs) have been widely studied and are technologically mature, they still suffer from many drawbacks: corrosion or the complexity of the cycles to achieve high temperature lifts [5,6]. Compared to absorption systems, Thermochemical Heat Transformers (THT) (using a solid/gas chemical reaction) are far from being technologically mature and have not been extensively studied to date. Nevertheless, few studies have shown the potential of this technology [7–13], highlighting their potential to obtain high temperature lift (> 50 °C), using a simple system architecture and without crystallization or corrosion problems [10].

As presented more in details in section 2.2, 1-salt or 2-salts cycles (also called resorption cycle) are mainly used in THT, water and ammonia being the most common working fluids. In these systems, salt/ammonia couples have been the most widely studied [10,14–18]. Other couples, such as salt/methanol, salt/CO_2 and salt/H_2O have been studied, with encouraging results for the latter two [19–22]. Among these couples, those using water vapor as reactive gas seem to be very suitable for THT applications in industry (low cost, non-toxicity), $CaCl_2$ being one of the most interesting salt candidate [13,23].

Currently, one of the main drawbacks of sorption systems in general and THTs in particular, is the solid reactive material implementation. Although many studies have been carried out, the use of bed of pure material presents many disadvantages, such as heat and mass transfer limitations, performance degradation due to microstructure change, melting and aggregation after excess hydration, etc. [24,25]. In order to limit these problems, different approaches have been studied.

Most of them focus on increasing the heat and mass transfer parameters by improving the heat exchanger or confining the reactants in a matrix (expanded natural graphite, metallic foams, adsorbents, etc.), thus obtaining composite materials with improved mass and heat transfer parameters [26].

For THT applications, Esaki et al. [9] experimented a packed bed reactor containing around 500 g $CaCl_2$. Different reactor designs have been considered to evaluate the impact of various devices to

enhance the heat (addition of fins) and mass transfer (addition of a vapor diffuser) in the packed bed. Significant gain was achieved by improving both transfers, the mean specific power increasing from 106 to 293 kW/m^3. Stengler and Linder [25] introduced a tree-like exchanger structure to enhance thermal conductivity of a salt bed of $SrBr_2$. The same authors performed a numerical thermal sensitivity analysis on the same geometry [27]. They concluded that after enhancement of the thermal conductivity of the bed, a further way of improving performances is to increase the heat transfer coefficient between reactive solid and heat exchanger. A more recent work performed by Esaki and Kobayashi [28] proposes a comparison of the impact of packed bed width, use of compound material (powdered $CaCl_2$, 300-500 µm in particle size, and expanded graphite with particle diameter of 7 µm in average) and water vapor diffuser (porous Ni plate inserted in the middle of the packed bed channel). While the reactor filled the compound material performs slightly better than its equivalent filled only with salt, the highest peak performances in terms of temperature and specific power are achieved for the reactor with the lowest channel width (2 mm). However, the configuration with a 4 mm width channel, exhibits more flat evolutions of the reactor temperature and specific power which could be more interesting for the development of a complete heat transformer. For the largest width (8 mm), the drop in specific power is noticeable with a constant decrease of about 25% compared to the 4 mm case. This work highlights clearly that heat transfer limitation due to reactant thickness is the main cause of performance limitation but also that a trade-off has to be found between the achievement of high peak performance and more stable ones.

A possible way to improve the heat transfer is to deposit a layer of reactive solid (of micrometric to millimetric thickness) directly on the surface of the heat exchanger. Some studies have been carried out, mainly for adsorbents dedicated to cooling applications and promising results have been obtained [29–32]. Thus, high specific power, up to several hundred W/kg, have been measured [29] and confirmed recently by McCague et al. [33]. However, as highlighted recently by He et al. [34] and by Venegas et al. [35] the coating method and the binder content and behavior can highly impact the performance.

Despite the high potential benefit that can be expected from the direct coating of the reactant material on the heat exchanger for THT applications, this approach has only been scarcely explored so far to the best knowledge of the authors. For example, in recent reviews on thermochemical systems [36,37], the focus is clearly put on heat storage applications for which coating is considered as a possible way to contain the reactant in a matrix (e.g. [38]) rather than as a way to deposit it at the surface of a heat-exchanger for heat-pumping applications.

Hence, the paper main contribution lies in taking a first step forward in developing a salt-coated heat exchanger for high temperature of thermochemical heat transformers (i.e. for applications such as waste heat upgrade in the industry). This is achieved by experimentally assessing the performance of a THT using water vapor as reactive gas and $CaCl_2$ as reactive solid, for operating temperature up to 150 °C (heat supply to the industrial process) and temperature lift between 40 and 80 K. Two configurations are tested: a reference one representative of a packed bed, i.e. a thick layer of salt in contact with a model heat exchanger plate and one with a deposit of $CaCl_2$/PVA (PolyVinyl Alcohol used as binder) to model a coated reactor. After a brief description of the developed experimental test bench, the dynamic behavior of the two configurations during hydration is compared and the impact of operating conditions assessed. Repeatability experiments, to assess the ageing of the deposit, are discussed. Finally global performances are compared to values available in the literature.

2. Principle of solid/gas sorption processes for thermochemical heat transformer

2.1 Solid/gas reaction for thermochemical heat transformer

The thermochemical heat transfer involves a monovariant reversible chemical reaction between a solid and a gas:

$$S + \nu G \leftrightarrows S' + \nu \Delta h_r^0 \quad (1)$$

The equilibrium conditions (p_{eq}, T_{eq}) of this solid/gas reaction follow the Clausius-Clapeyron relation (equation 2). Assuming the reactive gas follows an ideal gas behavior, the thermodynamic equilibrium conditions are determined by only one intensive variable: the equilibrium pressure p_{eq} or the equilibrium temperature T_{eq}:

$$p_{eq} = p^0 e^{-\frac{\Delta h_r^0}{RT_{eq}} + \frac{\Delta s_r^0}{R}} \quad (2)$$

p^0 is the reference pressure (1 bar), Δh_r^0 and Δs_r^0 are respectively the standard enthalpy and entropy of reaction.

2.2 Operating of thermochemical heat transformers

Among the operating cycles of THT using water as working fluid, the 1-salt and 2-salts are the two main configurations [10]. The 1-salt cycle consists of two reactors alternately connected to an evaporator and a condenser (see Fig. 1a). The cycle is described by a liquid/vapor equilibrium line (L/G line) and a solid/gas reaction equilibrium line (S/G line) in a Clapeyron diagram (see Fig. 1b). First, during the upgrade temperature phase waste heat (Q_{mLT}) at intermediate temperature (T_m at around 90 °C) is supplied to the evaporator allowing the water evaporation at "high pressure" P_h (e.g. 70 kPa for an evaporation temperature of 90 °C). This water vapor allows to realize the exothermic hydration reaction of the reactive material, releasing high-grade heat (Q_{HT}) at T_H. The temperature lift during this phase corresponds to the temperature difference between the intermediate temperature, T_m, and the high temperature, T_H: $\Delta T_{lift} = T_H - T_m$. The theoretical maximum temperature lift attainable by this system is achieved for adiabatic operation and corresponds to the temperature difference between the equilibrium temperature of the salt and the evaporation temperature at the "high pressure". In real systems, a gap from this value is necessary in order to obtain a suitable heat power from the reaction.

When the hydration reaction in the reactor finishes, the charging phase (or regeneration phase) of the reactor begins. Waste heat (Q_{mHT}) at T_m is supplied to the reactor while it is connected to a condenser maintained at low temperature (usually ambient temperature). This allows the reactive material dehydration at low pressure, P_L.

In order to decrease the required pressure lift when high temperature lifts are sought, Goetz et al. [39] proposed a 2-salts cycle, also called resorption heat pump. In this case, the evaporator and the condenser are replaced by two reactors filled with a so-called low temperature salt (see Figure 1c). In the Clapeyron diagram an S/G line has replaced the L/G line of the 1-salt configuration (Fig. 1d).

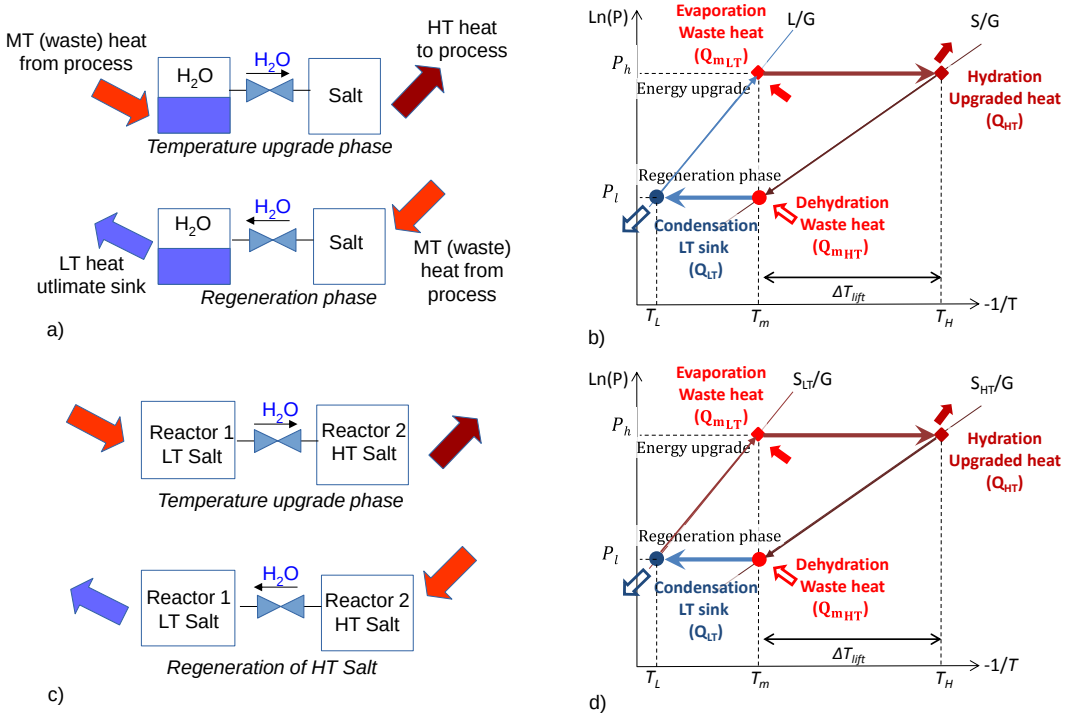

Figure 1: a) 1-salt THT working principle, b) 1-salt THT Clapeyron diagram. c) 2-salts THT working principle, d) 2-salts THT Clapeyron diagram (adapted from [13]).

3. Materials and methods

3.1 Experimental set up

An experiment was carried out to characterize the heat transfer and the kinetic reaction of reactive materials samples dedicated to THT application. The experimental setup is depicted in Figure 2. It is composed of two main elements: the reactor (2) and the Evaporator/Condenser (E/C) (1). Those two components are stainless steel tanks. The reactor is a double skin envelope tank of 350 mm inner diameter and 500 mm length, insulated with 1 cm of fiberglass. The E/C tank is a vessel of 200 mm inner diameter and 360 mm length insulated with 1.2 cm of Armaflex® foam. Their respective temperatures are controlled by two thermostatic baths. The "cold" thermal bath (IsoTemp 6200R28) (5) drives the temperature of the E/C using a spiral coil heat exchanger with an external area of around 0.025 m^2. The "hot" thermal bath (4 -Julabo HE-4) drives the flow in the reactor's double skin envelope and in a heat plate exchanger (HX) contained in the reactor (7). This reactor heat exchanger of 200 x 200 x 70 mm, enables to impose the temperature to the tested reactive sample (8). The vapor exchange between the reactor and the Evaporator/Condenser is carried out through a pipe with a diameter of 40 mm to minimize the pressure drop (3) and a ball valve. Both chambers are fitted with a ball valve for connection with a vacuum pump.

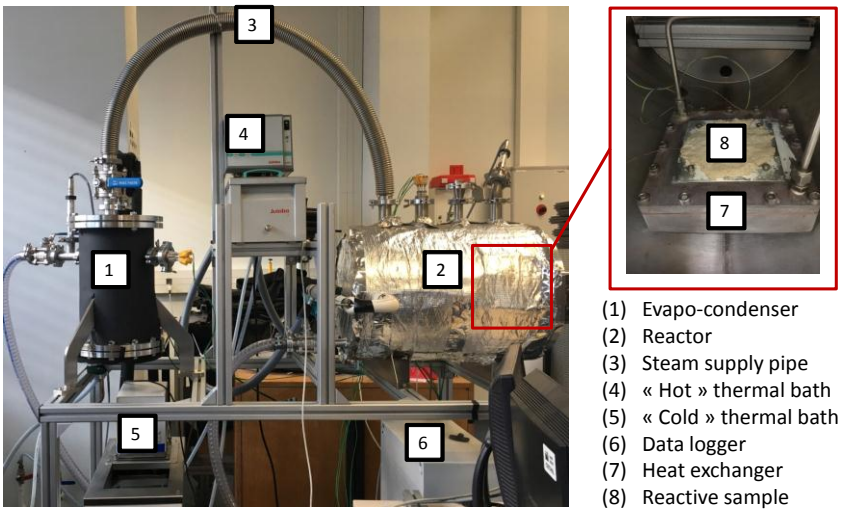

Figure 2: Photography of the experimental test bench

3.2 Instrumentation and measurement uncertainties

The experimental bench was thoroughly instrumented in order to monitor the progress of the thermochemical reaction. It is equipped with two pressure gauges (Keller PAA35X, 0-1 bar and 0-0.1 bar, uncertainty of 0.1 % of full scale) and ten thermocouples (TC, K-type), which were calibrated resulting in an accuracy estimated at ±0.2 °C. The different locations are detailed hereafter:

- Within the Evaporator/Condenser: the temperature of the liquid water and that of the heat transfer fluid inlet and outlet are measured. The water vapor pressure ($p_{v,E/C}$, ±100 Pa) is measured using the 0-1 bar pressure gauge.
- Within the reactor: five TC are located inside the reactor chamber. Two TC are set in the salt sample: one at the middle of the salt (T_s) and the other one ($T_{s/HX}$) at the bottom of the salt sample, at the interface between the salt and the heat plate exchanger (see Figure 3). Two other TC measure the vapor and the internal wall temperatures.

  The water vapor pressure ($p_{v,R}$, ±10 Pa) is measured using the 0-0.1 bar pressure gauge.
- At the inlet and outlet pipe of the reactor heat plate exchanger: two TC measure the temperature of the heat transfer fluid (thermal oil H20S, Julabo®).
- Additionally, the reactive samples are punctually weighed outside of the reactor (m_s, ±0.05g), to evaluate the reaction advancement (see section 4.2.1).

A NI-DAQ® acquisition unit (6) is used for the measures acquisition and measurements are recorded every 5 s.

3.3 Reactive material testing device

The choice of a suitable hydrate salt is an essential step in the conception of a thermochemical heat transformer. For the target application of upgrading temperature from around 100 °C to 150 °C, the calcium chloride has been identified as promising in a previous work [13]. While corresponding to a favorable operating temperature range, it also has the advantage to be non-toxic, low cost and to be easily available. In addition to the anhydrous form, the calcium chloride presents four stable hydrates: monohydrate, dihydrate, tetrahydrate and hexahydrate [40], which thermo-physical properties are listed in table 1.

In the present work, calcium chloride dihydrate powder was supplied by Sigma Aldrich® with purity higher than 99%.

Table 1. Properties of calcium chloride hydrates [40]

Hydrate	Molar mass ($g.mol^{-1}$)	Density ($kg.L^{-1}$)	Melting point (°C)
$CaCl_2$	111	2.16	773
$CaCl_2 \cdot H_2O$	129	2.24	187
$CaCl_2 \cdot 2H_2O$	147	1.85	176
$CaCl_2 \cdot 4H_2O$	183	1.83	45.3
$CaCl_2 \cdot 6H_2O$	219	1.47-1.8	28-30

As it can be seen on Figure 3, two salt configurations were tested. In the first one, a bed of pure salt is disposed over an aluminum plate of 10x10 cm^2 and 1 mm of thickness. The achieved bed thickness is about 20 mm (dihydrated mass between 60 and 80 g), using aluminum walls to prevent salt sewing from the plate (see Figure 3a). The low operating pressure (p_v < 55 kPa) and the double walled reactor allow to limit the edge effects. Moreover, the thermocouples are placed in the center of the reactive sample.

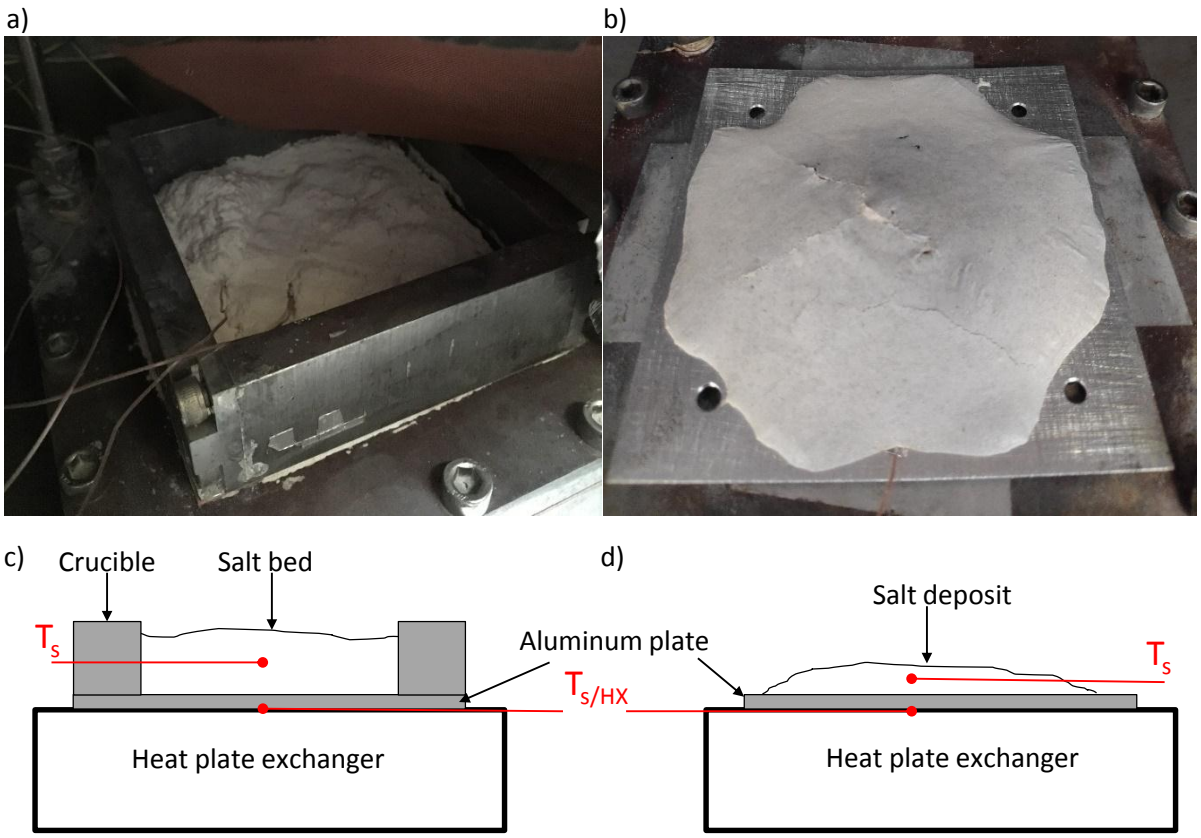

Figure 3: Photography of the two salt implementations studied and schema of the thermocouples locations: a) salt bed b) salt deposit c) TC repartition in the salt bed d) TC repartition in the salt deposit

The second configuration consists in a deposit on a thin aluminum plate (1 mm thick and 10x10 cm^2 square) of a compound material made of $CaCl_2$ and PVA (polyvinyl alcohol) as binder. To achieve this, distilled water and PVA are mixed together at 80 °C. Then the powder of dihydrate salt is added to the solution. It is stirred at 60 °C till full homogenization of the solution is reached. The solution is then deposited on the aluminum plate to obtain a deposit of around 1 cm thick (note that the thickness is not homogenous, it is of around 2 cm in the center and 0.5 mm on the border). The

distilled water is then evacuated from the deposit by heating in an autoclave oven during two days. Several temperature steps are conducted (50 °C, 100 °C, then 120 °C and finally 140 °C) to avoid the melting of the salt (the higher the water content, the lower the melting point as referred in table 1). At the end of the heating process, the reactive material is fully dehydrated and the final salt content of the deposit (in its dehydrated state) is 91 wt% for a total weight of around 20 g. During the deposit process, a thermocouple is placed in the solution before it dries. Another one is placed between the plate and the heat exchanger (figure 3d).

3.4 Experimental protocols

3.4.1 Solid-gas reactions equilibrium study

In order to determine the equilibrium reaction conditions of the different calcium chloride hydrates, the following protocol has been used.

The different experiments conducted to determine the equilibrium relations of the $CaCl_2/H_2O$ reactions have been realized with around 80 g of dihydrated salt implemented in packed bed and placed on the reactor heat plate exchanger. The sample was initially dehydrated and then set to the desired initial conditions. Initial salt temperature was 160 °C. The range of initial vapor pressures, fixed by controlling the E/C temperature, varied between 3 and 30 kPa. The initial pressure is chosen so that the salt still is in anhydrous state. The reactor is disconnected to the E/C and progressively cooled down to start the hydration reaction. The temperature is decreased till 40 °C and increased back to 160 °C in order to complete a full hydration-dehydration cycle. If temperature varies slowly enough, it can be considered that the salt is always at equilibrium. Different heating rates have been tested: 0.5 K/min, 0.2 K/min, 0.1 K/min and 0.05 K/min. Experimental results has shown that the decrease of the heating rate has no more influence below 0.1 K/min. Hence, this heating rate has been chosen for all the studies of the reaction equilibrium conditions.

3.4.2 Hydration study

In order to investigate the reactive samples performances (temperature lift, reaction kinetics, cycle stability, etc.) under variant representative operating conditions of a 1-stage 1-salt THT configuration, the following experimental protocol has been carried out.
The reactive sample is firstly dehydrated and weighed. During the hydration step, the waste heat temperature T_m is imposed to the E/C using the cold bath, while the high temperature bath is used to impose the high temperature T_H of the salt heat plate exchanger.
In order to follow the reaction advancement, weighing is performed. In this case, the E/C and the reactor are disconnected. The salt is weighed on the scale outside of the reactor. It is then reintroduced inside the reactor and vacuum is made during ten minutes using a vacuum pump. The E/C is then reconnected to the reactor to continue the hydration reaction.

4. Results and discussion

4.1 Solid-gas equilibriums characterization

The $CaCl_2$/water reactions equilibriums are important data for thermochemical systems design. Several characterization attempts are found in the literature (see Figure 5), however some references are divergent [40–43]. The hydration reactions allowing to go from the anhydrous calcium chloride to the dihydrate calcium chloride (i.e. the reaction from $CaCl_2$ to $CaCl_2 \cdot 1H_2O$ and the reaction

from $CaCl_2 \cdot 1H_2O$ to $CaCl_2 \cdot 2H_2O$) have been experimentally investigated using the method described in the section 3.4.2 in order to determine the corresponding equilibrium relations.

Hydration reaction from anhydrate to dihydrated state of the calcium chloride is plotted on Figure 4. At first, the pressure decreases linearly with temperature, the salt being initially anhydrous, it cannot react until its temperature reaches the first reaction equilibrium curve (between the anhydrous and the monohydrated state, i.e. $CaCl_2$ to $CaCl_2 \cdot 1H_2O$ reaction). During this step, pressure and temperature of the vapor are linked, following an ideal gas behavior, as shown on Figure 4. When the imposed salt temperature reaches the first reaction equilibrium, the salt hydrates consumes water which decreases the reactor pressure following the hydration reaction from $CaCl_2$ to $CaCl_2 \cdot 1H_2O$ equilibrium line. Once the fully monohydrated state is reached, the salt cannot be hydrated anymore. Further decrease of the salt temperature leads to reaching the second reaction equilibrium: from $CaCl_2 \cdot 1H_2O$ to $CaCl_2 \cdot 2H_2O$, the water vapor following an ideal gas behavior. There, the second equilibrium line is followed until saturation. Note that the pressure oscillations observed at high pressure and temperature are due to vapor condensation/evaporation on the wall of the reactor.

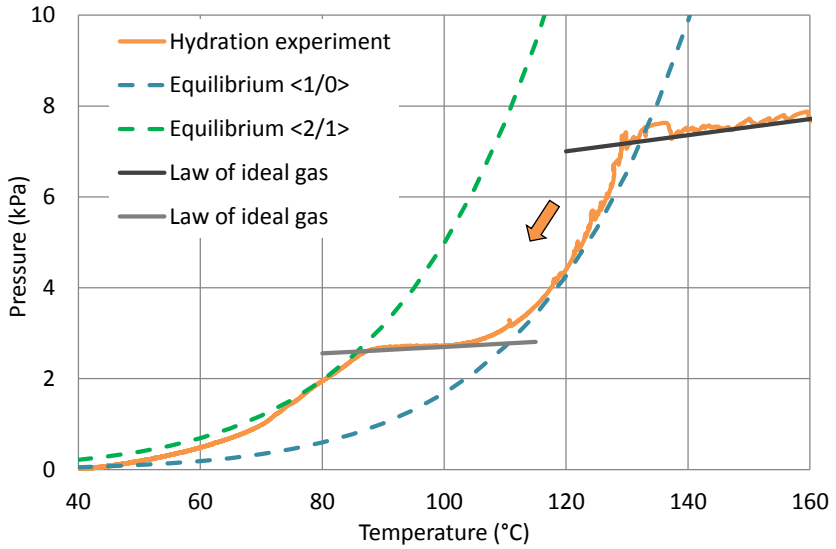

Figure 4: Hydration reaction from anhydrate to dihydrated state of the calcium chloride. Equilibrium lines are from the experimental study presented section 4.1.

By changing the initial conditions (i.e. initial vapor pressure), it is then possible to determine the salt equilibriums in a wide range of pressure and temperature. The coefficients of the Clausius-Clapeyron equilibrium reaction equations have been determined using minimization function with differential evolution method. The obtained results are presented in the Figure 5 and compared to results from the literature [23,40–43]. The lines represent the experimental fitted curves and the markers represent the experimental range of measurements. The fitted equations for each reaction, both from this work and literature, are listed in annex (table A1).

Although the obtained equilibriums are close to those of the literature, differences have been highlighted. Thus, Molenda et al. [41] have identified non stoichiometric reactions between the anhydrous and dehydrate calcium chloride: $CaCl_2$ to $CaCl_2 \cdot 0.3H_2O$ reaction and $CaCl_2 \cdot 0.3H_2O$ to $CaCl_2 \cdot 2H_2O$ reaction. However, since no mass tracking has been realized in this study, no conclusion can be done about the presence of these reactions. Complementary TGA-DSC analysis should be done to determine the exact hydration state reached.

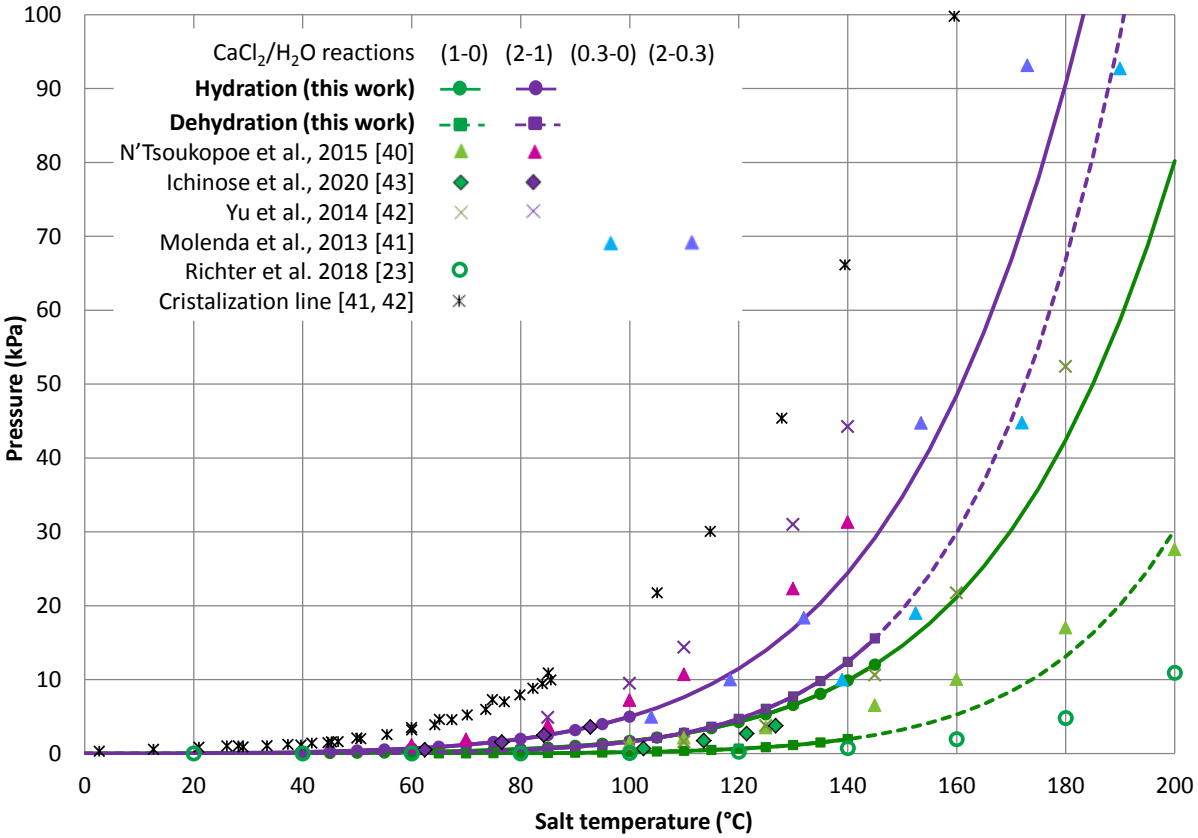

Figure 5: Dehydration and hydration equilibrium line of $CaCl_2$ hydrate. For the data from this work, the lines correspond to the fit with the Clausius-Clapeyron relation and the markers correspond to the experimental range studied [23,40–43].

Furthermore, contrarily to the data from the literature, a hysteresis phenomenon between hydration and dehydration reaction is observed, the larger effect being for the reaction (CaCl2 to CaCl2·1H2O reaction). In the perspective of the THT application, this hysteresis is unfavorable as it will require a lower pressure (i.e. a lower "low temperature") to achieve CaCl2 dehydration during the regeneration phase. Different phenomena could explain this hysteresis. Firstly, as observed by Molenda et al. [41], the determination of the thermodynamic equilibrium in a dynamic way can conduct to overestimate the reaction temperature (for a given vapor pressure) in dehydration and underestimate this temperature in hydration. Indeed, due to the heat and mass transfer resistances inside the salt, the effective temperature hardly corresponds to the targeted operating conditions (temperature or vapor pressure). This phenomenon is all the more important as the heating rate is high. However, in our case a heating rate study has shown that no more impacts on the equilibrium are observed for heating rate equal or inferior to 0.1 K/min. Sögütoglu et al. [44] highlighted another phenomenon called "induction time" that could explain the observed hysteresis. They reported that for some salts there is an inactive metastable zone around the equilibrium were a time is necessary to start the reaction. They explain this induction time due to the presence of a nucleation barrier. The reaction must be therefore initiated far enough away from the equilibrium in order to create a first nucleation of the new hydrate and start the reaction. To investigate this hypothesis with the calcium chloride, a cycle starting from an incomplete hydration has been realized in order to start the dehydration with sample containing monohydrated (CaCl2·1H2O) and anhydrous calcium chloride (Figure 6). No impact of the incomplete hydration is identified on the hysteresis so that the presence of nucleation barrier was not highlighted in the present case. Further investigations have to be performed to better understand the origin of the observed hysteresis phenomenon.

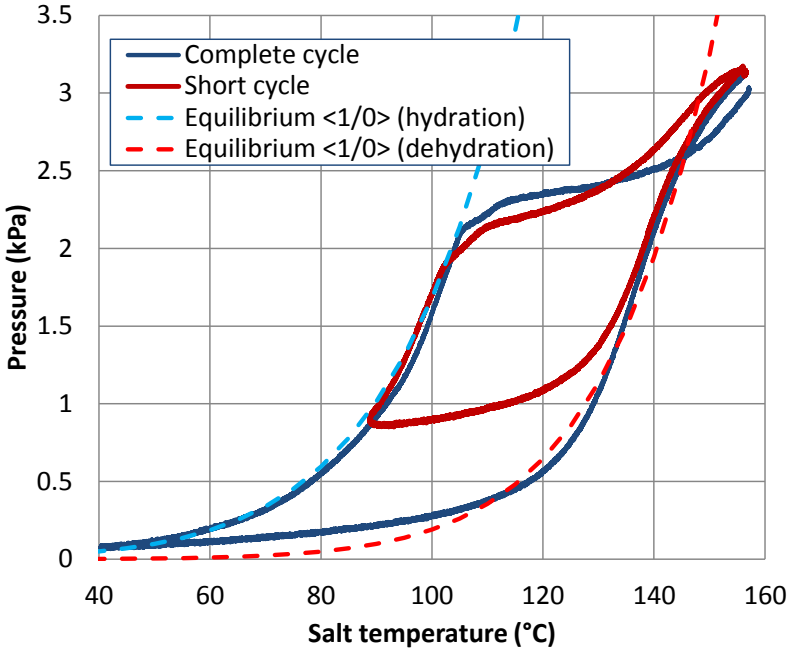

Figure 6: Comparison between short and long cycle

4.2 THT performances analysis

This part aims at analysing the dynamic behavior and the performances of packed bed and deposit implementations of salt for a 1-salt THT configuration. Several hydrations were conducted with different realistic operating conditions and salt implementation (packed bed or deposit). All the obtained results are summarized in table A2.

4.2.1 Dynamic behavior

The reactive sample temperature evolutions of a typical hydration experiment for packed bed and deposit implementations are presented on the Figure 7a and b, respectively.

Figure 7a shows that as vapor is injected, salt temperature rises rapidly with the beginning of the exothermic hydration reaction. A bulk salt temperature over 173 °C is reached, meanwhile the peak temperature in the bottom of the crucible does not excess 168 °C. Then, a first salt temperature plateau, at around 170 °C, is observed during around 20 min, followed by a second temperature plateau at lower temperature (around 150 °C) during two hours. Finally, the salt temperature decreases gradually to reach temperature close to the heat transfer fluid temperature (139 °C). Due to the heat losses, salt temperature lower than the inlet heat transfer fluid temperature ($T_{i,htf}$) are observed at the end of the experiment. The two rapid falls of temperatures and pressure correspond to the punctual weighing of the reactive bed.

In agreement to the equilibrium temperatures of the two first hydration reactions of the calcium chloride (T_{eq} *(0-1)* and T_{eq} *(1-2)*), the salt bed temperature plateaus correspond to the two first hydration reactions of the $CaCl_2$: $CaCl_2$ to $CaCl_2{\cdot}1H_2O$ reaction and $CaCl_2{\cdot}1H_2O$ to $CaCl_2{\cdot}2H_2O$ reaction. When the first exothermal reaction is complete at the thermocouple emplacement, the salt temperature decreases to tend to the equilibrium temperature of the second reaction. Finally, when the second exothermal reaction is complete, the salt temperature reaches the imposed bottom plate temperature (i.e. the inlet heat transfer fluid temperature).

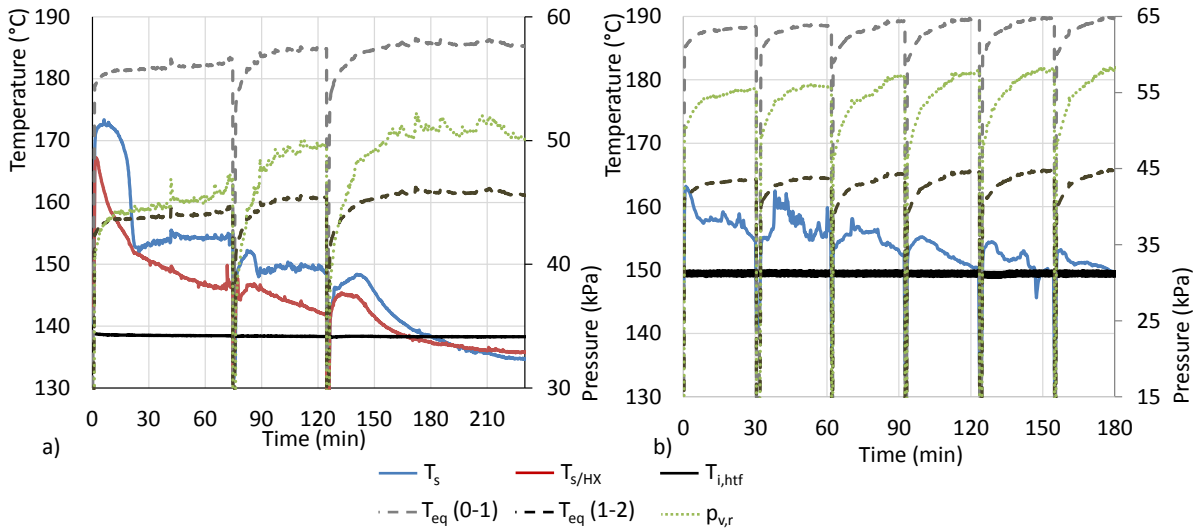

Figure 7: Pressure and temperature evolution a) of the 1-salt hydration with a packed bed implementation (sample 1: T_m/T_H = 78.6/138.7 °C); b) of the 1-salt hydration with a deposit implementation (sample 12: T_m/T_H = 81.8/148.9 °C).

For the coated plate, (Figure 7b) a lower salt peak temperature is observed (153 °C) and no plateau occurs. The heat transfer fluid temperature is also reached more rapidly. This reflects directly the decrease in heat transfer resistance with this configuration.

The average reaction advancement, calculated from the equation (3) is presented on Figure 8 for both configurations. X corresponds to the average number of mole of water contain in the reactive material per mole of salt. It is equal to 0 in the anhydrous state, 1 for the $CaCl_2 \cdot 1H_2O$, etc.

$$X = \frac{(m_{s,0} - m_s) M_{CaCl2}}{M_v m_{s,0}} \quad (3)$$

m_s is the mass of salt and $m_{s,0}$ is the mass of dehydrated salt, i.e. initial mass of salt.

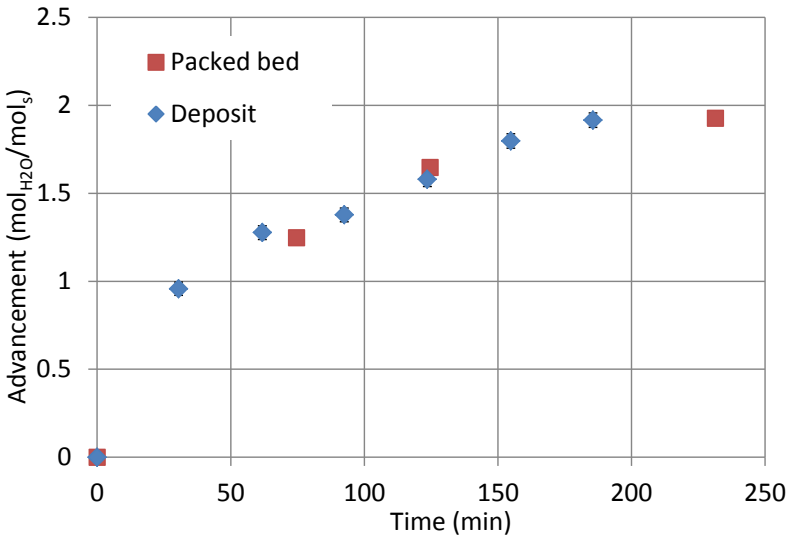

Figure 8: Reaction advancement vs. time of the 1-salt hydration with a packed bed (sample 1: T_m/T_H = 78.6/138.7 °C) and deposit (sample 12: T_m/T_H = 81.8/148.9 °C) implementations.

For packed bed configuration, in accordance to the salt bed temperature evolution, the average reaction advancement presented in the Figure 8 shows that both the $CaCl_2$ to $CaCl_2{\cdot}1H_2O$ and $CaCl_2{\cdot}1H_2O$ to $CaCl_2{\cdot}2H_2O$ hydration reactions have been achieved.
Similar results are obtained for the deposit configuration. Moreover, comparable reaction time are observed between the two different implementation though in the case of the deposit, the operating conditions are less favourable (T_H = 148.9 °C instead of 138.7 °C for the packed bed experiment). This shows that the deposit implementation allows to enhance the heat and mass transfer inside the reactive material and therefore the reaction kinetic.

4.2.2 Sensitivity to the thermal sources temperature

For each salt implementation, this sensitivity analysis focuses on the salt temperature and reaction kinetic evolutions for different waste heat temperature (T_m) and released heat temperature (T_H). The comparison of three hydration experiments of around one hour (reference case (red), lower T_H case (blue) and higher T_m case (green)) are presented in the Figure 9a and b respectively for the packed bed and the deposit implementations.

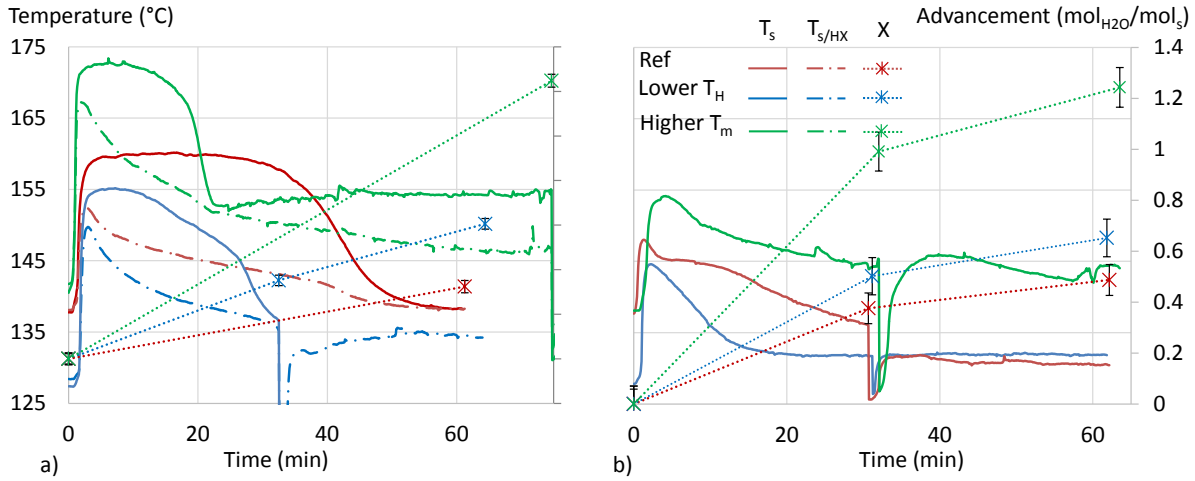

Figure 9: Salt temperature and reaction advancement evolutions for different operating temperatures (T_H and T_m);
a) packed bed implementation ("reference" case (sample 6): T_m/T_H = 62.9/138.5 °C, "lower T_H" case (sample 8): T_m/T_H = 61.5/126.5 °C, "higher T_m" case (sample 1): T_m/T_H = 78.6/138.7 °C);
b) deposit implementation ("reference" case (sample 13): T_m/T_H = 60.5/130.9 °C, "lower T_H" case (sample 15): T_m/T_H = 60.7/128.4 °C, "higher T_m" & T_H case (sample 10): T_m/T_H = 70.4/138.6 °C).

For both salt implementations, change in T_H affects the salt peak temperature. It decreases by about 5 °C (from 160 °C to 155 °C) when reducing T_H by 12 °C in the packed bed and it decreases by 3.5 °C (from 148 °C to 144.5 °C) when reducing T_H from 131 °C to 128.4 °C for the deposit implementation. Although the reaction temperature is imposed by the vapor pressure and therefore by the waste heat temperature, these peak temperature differences can be explained by several phenomena: the higher heat transfer due to the lower heat plate exchanger temperature (T_H); the different salt initial temperatures (imposed at T_H). Furthermore, as the heat transfer and the equilibrium drop are higher for hydration with lower T_H, the reaction kinetics increases when reducing the heat released temperature.
Increasing the waste heat temperature T_m leads to an increase of the system vapor pressure and therefore an important increase of the peak temperature and of the plateau temperatures of each hydration reactions ($CaCl_2$ to $CaCl_2{\cdot}1H_2O$ reaction and $CaCl_2{\cdot}1H_2O$ to $CaCl_2{\cdot}2H_2O$ reaction) is observed

for both salt implementations (green lines on Figure 9). Moreover, similarly to sensitivity study of T_H, the increase of T_m leads to an increase of the equilibrium deviation and therefore to the reaction kinetic. It can also be observed that the system is more sensitive to the intermediate temperature T_m than to T_H. Indeed, as shows Figure 9b, though the higher T_m case of the deposit implementation presents also a higher T_H of the same order of magnitude (around 10 K) compared to the reference case, an important increase of the reaction kinetic is still observed.

4.2.3 Repeatability

Hydration/dehydration cycles at identical operating conditions have been done for both salt implementations. In order to fully dehydrated the reactive material between each cycle, dehydration with extreme operating conditions (T_L/T_H = 2/150 °C) have been conducted. No mass monitoring has been conducted for these experiments to avoid the resulting disturbances. Four cycles have been realized with the deposit implementation and due to the higher reaction time with the packed bed implementation only two cycles have been conducted.

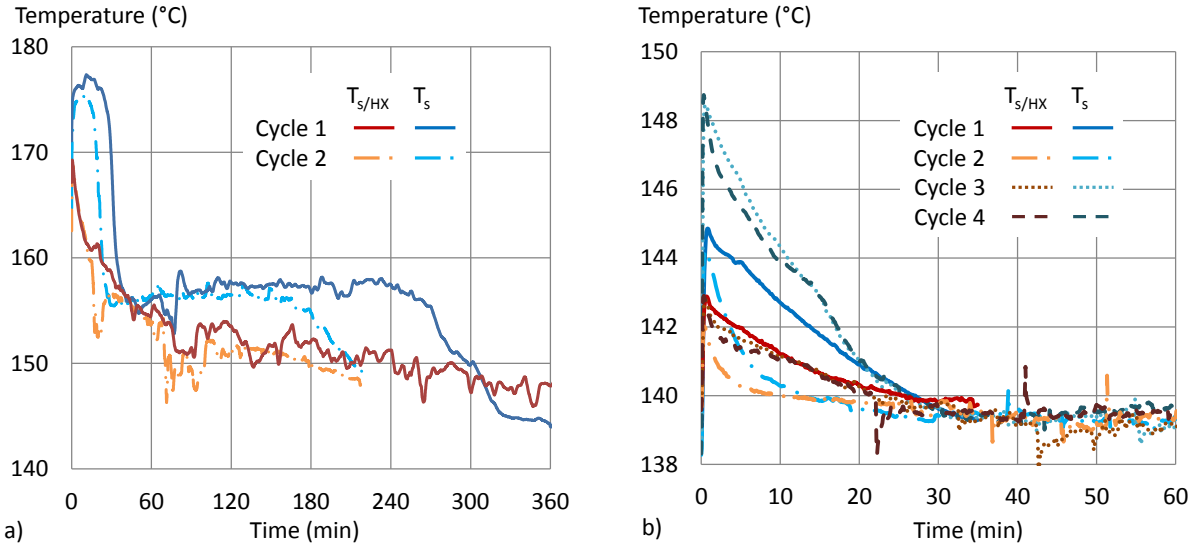

Figure 10: Salt temperature evolutions during hydration for few hydration/dehydration cycles at identical operating conditions; a) packed bed implementation (sample 9: $T_L/T_m/T_H$ = 2/80.5/147.4 °C); b) deposit implementation (sample 16: $T_L/T_m/T_H$ = 2/66.1/138 °C).

Figure 10a and b present respectively the salt temperature evolution during hydration for the two cycles with the packed bed implementation and the four cycles with the deposit implementation.
For the packed bed implementation, no significant changes on the level of temperature peaks and plateaus are observed. However, the salt temperatures of each plateau decrease quicker for the second cycle. This indicates that the hydration reactions are finished earlier at the thermocouple location during the second cycle. It can be due to a faster reaction kinetic or a displacement of the thermocouple in the packed bed due to the reactive bed deformation during hydration/dehydration reaction.

For the deposit implementation, the temperature time course changes during the two first cycles and seems to be stabilized after the third cycle, with a peak of temperature increasing from 145 °C during the cycles 1 and 2 to over 148 °C for the two last cycles.
These temperature evolutions can be explained by the deposit ageing during cycles. After few cycles, cracks and problems of adhesion to the heat exchanger appear for the deposit configuration (Figure

11). This can lead higher thermal resistance that can explain the increase of the peak temperature. Furthermore, from the cross-sectional view (Figure 11c), a potential segregation between the salt and the binder is observed, potentially resulting in a drop in performances. Hence, it can be concluded that further development is needed to limit the ageing of the salt/binder compound and improve its adhesion on the heat exchanger surface.

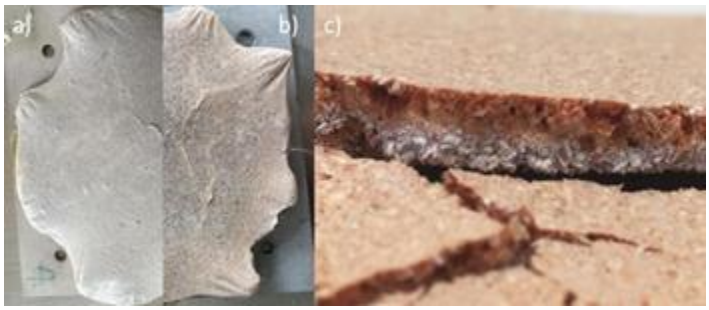

Figure 11: Picture of a PVA-deposit a) before experiment and b) after one hydration-dehydration cycle at $T_L/T_m/T_H$ = 2/65.9/138.1 °C (sample 16) and c) after four cycles.

4.2.4 Global performances

The THT performance directly depends on the kinetic reaction. The impact of the waste heat temperature (70 °C < T_m < 100 °C) and of the demand temperature (130 °C < T_H < 160 °C) is assessed for the two THT implementation (packed bed and deposit). Three criteria are evaluated:

1. The average specific heating power during the first hydration reaction ($CaCl_2$ to $CaCl_2{\cdot}1H_2O$ reaction). This parameter is calculated using the salt mass variation during the first hydration reaction and the corresponding reaction enthalpy $\Delta h^0_{r\,(0-1)} = 73360$ J/mol$_v$ [23]:
   $$q_m = \frac{(m_{s,0}-m_s)}{M_v m_{s,0} \Delta t} \Delta h^0_{r\,(0-1)} \quad (4)$$
   With Δt the time between the measure of m_s and the beginning of the $CaCl_2$ to $CaCl_2{\cdot}1H_2O$ hydration reaction.
2. The thermodynamic driving force. Any change in the operating conditions (T_L, T_m, T_H) results in a change in equilibrium drop. This can be related to the thermodynamic driving force of the reaction [13,45]. Usually the greater the driving force, the greater the reaction kinetic. For pure substances and ideal mixtures, the driving force can be described by the Gibbs free energy of the reaction and can be written as:
   $$F_m = \frac{\Delta g_r}{\nu RT} = \ln\left(\frac{p_v}{p_{eq}(T)}\right) \quad (5)$$
3. The temperature lift, that corresponds to the temperature increase:
   $$\Delta T_{lift} = T_H - T_m \quad (6)$$

Note that the presented values of the driving force and temperature lift are average values during the hydration reaction.

Figure 12 presents the average specific power released by the samples as function of the driving force. A large range of average specific power is obtained, between 36 W/kg and 341 W/kg. This figure shows that the specific power depends to the driving force of the reaction. As it has been already observed numerically [13], for a given salt implementation (corresponding to given heat and mass transfer parameters inside the reactive material) the specific power increases with the driving force. This parameter is therefore an interesting parameter allowing to obtain rapidly an estimate of

the system performances. Furthermore, for a given driving force the deposit implementation leads in general a higher average specific power than for the packed bed implementation. This highlights the benefit of this configuration in terms of heat and mass transfer enhancement. Nevertheless, the few numbers of tested samples and the discrepancy observed for the results with the deposit implementation cannot allow to define a clear relation between the average specific power and the driving force. This performances variability can be explained by possible degradation (formation of cracks, problems of deposit adhesion, etc.) of the deposit sample during the hydration reaction (see section 4.2.3).

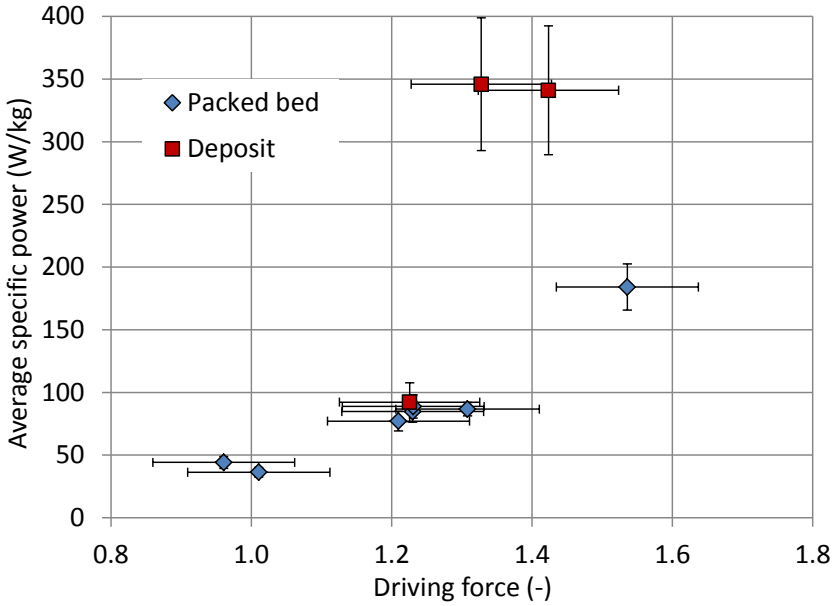

Figure 12: Average specific power vs. driving force for two salt implementations (packed bed and deposit.

The impact of the imposed temperature lift on the average specific power is presented in the Figure 13 for the two salt implementations and for different experimental results from the literature (for 1-salt THT configuration). This figure shows that, in a general way the specific power decreases when the temperature lift increases (due to the decrease of the equilibrium drop).

For a packed bed implementation, the obtained results are comparable to that of the literature with a specific power of around 180 W/kg obtained for a temperature lift of 60 K. Although discrepancy is observed with the results of the deposit implementation, Figure 13 shows that with the same THT configuration the deposit implementation can allow to obtain better performances than the packed bed implementation. Thus, for the same temperature lift, performances higher than the one obtained with the packed bed implementation and the one obtained in the open literature are reached with the deposit implementation, with average specific power until 341 W/kg for a temperature lift of 67 K.

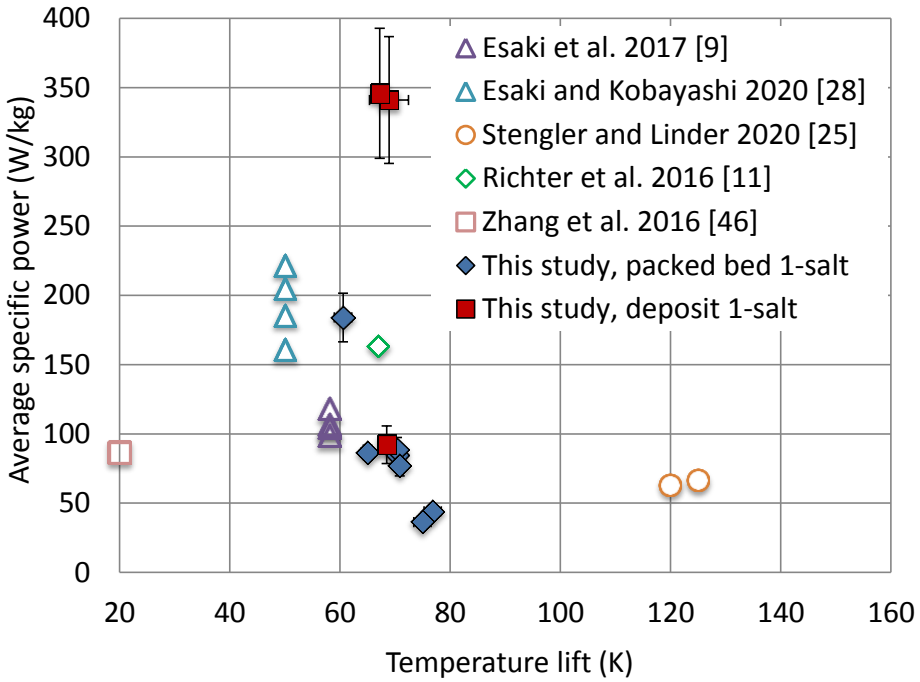

Figure 13: Average specific vs. temperature lifts for different thermochemical systems from this work and the literature [9,11,25,28,46].

5. Conclusion

In this paper, two reactor configurations for thermochemical heat transformers applications for industrial waste heat recovery are evaluated: a packed bed one and a coated heat exchanger. In both cases, $CaCl_2$/water is used as working pair while the reported work is restricted to the hydration step (i.e. heat generation at required process demand).

For the packed configuration, the temperature evolution is characterized by a peak of temperature at reaction beginning, followed by a plateau and a decrease towards reaching the secondary fluid temperature. For the coated heat exchanger configuration, the peak occurs as well, but with a lower amplitude and the plateau is replaced by a decay towards the secondary fluid temperature. This behavior reflects directly the decrease in heat transfer resistance for the second configuration.

The performance is assessed using the average specific power and the temperature lift obtained for the first hydration reaction ($CaCl_2$ to $CaCl_2 \cdot 1H_2O$ reaction) for different operating conditions (T_m and T_H). Compared to packed bed, the deposit configuration allows to significantly increase the THT performances with a specific power increasing from 180 W/kg to 341 W/kg for a temperature lift of around 60 K. High sensitivity to temperature lift is also observed with for example a decrease from 140 W/kg to 38 W/kg when ΔT_{lift} increases from 60 K to 77 K for the packed bed implementation. Finally, ageing of the deposit is identified during repeatability experiments leading in a drop in performance (i.e. increase in peak temperature corresponding to an increase in heat transfer resistance due to cracks and partial deposit detachment)

To complete this work, it would be interesting to extend the proposed methodology to the study of the regeneration phase (salt dehydration), to test the deposit implementation at a larger scale. Work as also to be performed to progress in the coating formulation and behavior characterization, in order to improve the deposits durability.

ACKNOWLEDGEMENT

The authors wish to thank the INSA LYON (BQR FATAL RECUP) for funding this study.

References

[1] Forman C, Muritala IK, Pardemann R, Meyer B. Estimating the global waste heat potential. Renew Sustain Energy Rev 2016;57:1568–79. https://doi.org/10.1016/j.rser.2015.12.192.

[2] Xu ZY, Wang RZ, Yang C. Perspectives for low-temperature waste heat recovery. Energy 2019;176:1037–43. https://doi.org/10.1016/j.energy.2019.04.001.

[3] Zhang H, Baeyens J, Cáceres G, Degrève J, Lv Y. Thermal energy storage: Recent developments and practical aspects. Prog Energy Combust Sci 2016;53:1–40. https://doi.org/10.1016/j.pecs.2015.10.003.

[4] Arpagaus C, Bless F, Uhlmann M, Schiffmann J, Bertsch SS. High temperature heat pumps: Market overview, state of the art, research status, refrigerants, and application potentials. Energy 2018;152:985–1010. https://doi.org/10.1016/j.energy.2018.03.166.

[5] Zhang J, Zhang H-H, He Y-L, Tao W-Q. A comprehensive review on advances and applications of industrial heat pumps based on the practices in China. Appl Energy 2016;178:800–25. https://doi.org/10.1016/j.apenergy.2016.06.049.

[6] Parham K, Khamooshi M, Tematio DBK, Yari M, Atikol U. Absorption heat transformers – A comprehensive review. Renew Sustain Energy Rev 2014;34:430–52. https://doi.org/10.1016/j.rser.2014.03.036.

[7] Li T, Wang R, Kiplagat JK. A target-oriented solid-gas thermochemical sorption heat transformer for integrated energy storage and energy upgrade. AIChE J 2013;59:1334–47. https://doi.org/10.1002/aic.13899.

[8] Wu S, Li TX, Yan T, Wang RZ. Experimental investigation on a novel solid-gas thermochemical sorption heat transformer for energy upgrade with a large temperature lift. Energy Convers Manag 2017;148:330–8. https://doi.org/10.1016/j.enconman.2017.05.041.

[9] Esaki T, Yasuda M, Kobayashi N. Experimental evaluation of the heat output/input and coefficient of performance characteristics of a chemical heat pump in the heat upgrading cycle of CaCl2 hydration. Energy Convers Manag 2017;150:365–74. https://doi.org/10.1016/j.enconman.2017.08.013.

[10] Yu YQ, Zhang P, Wu JY, Wang RZ. Energy upgrading by solid–gas reaction heat transformer: A critical review. Renew Sustain Energy Rev 2008;12:1302–24. https://doi.org/10.1016/j.rser.2007.01.010.

[11] Richter M, Bouché M, Linder M. Heat transformation based on CaCl2/H2O – Part A: Closed operation principle. Appl Therm Eng 2016;102:615–21. https://doi.org/10.1016/j.applthermaleng.2016.03.076.

[12] Stengler J, Bürger I, Linder M. Thermodynamic and kinetic investigations of the SrBr2 hydration and dehydration reactions for thermochemical energy storage and heat transformation. Appl Energy 2020;277:115432. https://doi.org/10.1016/j.apenergy.2020.115432.

[13] Michel B, Clausse M. Design of thermochemical heat transformer for waste heat recovery: Methodology for reactive pairs screening and dynamic aspect consideration. Energy 2020;211:118042. https://doi.org/10.1016/j.energy.2020.118042.

[14] Manente G, Ding Y, Sciacovelli A. Organic Rankine cycles combined with thermochemical sorption heat transformers to enhance the power output from waste heat. Appl Energy 2021:117980. https://doi.org/10.1016/j.apenergy.2021.117980.
[15] Jiang L, Wang RQ, Tao X, Roskilly AP. A hybrid resorption-compression heat transformer for energy storage and upgrade with a large temperature lift. Appl Energy 2020;280:115910. https://doi.org/10.1016/j.apenergy.2020.115910.
[16] Wu S, Li TX, Yan T, Wang RZ. Advanced thermochemical resorption heat transformer for high-efficiency energy storage and heat transformation. Energy 2019;175:1222–33. https://doi.org/10.1016/j.energy.2019.03.159.
[17] Hinmers S, Atkinson GH, Critoph RE, van der Pal M. Resorption Thermal Transformer Generator Design. Energies 2022;15:2058. https://doi.org/10.3390/en15062058.
[18] Hinmers S, Atkinson GH, Critoph RE, van der Pal M. Modelling and Analysis of Ammonia Sorption Reactions in Halide Salts. Int J Refrig 2022;137:188–211. https://doi.org/10.1016/j.ijrefrig.2022.01.032.
[19] Wongsuwan W, Kumar S, Neveu P, Meunier F. A review of chemical heat pump technology and applications. Appl Therm Eng 2001;21:1489–519.
[20] Kato Y, Harada N, Yoshizawa Y. Kinetic feasibility of a chemical heat pump for heat utilization of high-temperature processes. Appl Therm Eng 1999;19:239–54. https://doi.org/10.1016/S1359-4311(98)00049-0.
[21] Kyaw K, Matsuda H, Hasatani M. Applicability of Carbonation/Decarbonation Reactions to High-Temperature Thermal Energy Storage and Temperature Upgrading. J Chem Eng Jpn 1996;29:119–25. https://doi.org/10.1252/jcej.29.119.
[22] Li W, Zhang L, Ling X. Thermo-economic assessment of salt hydrate-based thermochemical heat transformer system: Heat upgrade for matching domestic hot water production. Energy Convers Manag 2023;277:116644. https://doi.org/10.1016/j.enconman.2022.116644.
[23] Richter M, Habermann E-M, Siebecke E, Linder M. A systematic screening of salt hydrates as materials for a thermochemical heat transformer. Thermochim Acta 2018;659:136–50. https://doi.org/10.1016/j.tca.2017.06.011.
[24] Michel B, Mazet N, Mauran S, Stitou D, Xu J. Thermochemical process for seasonal storage of solar energy: Characterization and modeling of a high density reactive bed. Energy 2012;47:553–63. https://doi.org/10.1016/j.energy.2012.09.029.
[25] Stengler J, Linder M. Thermal energy storage combined with a temperature boost: An underestimated feature of thermochemical systems. Appl Energy 2020;262:114530. https://doi.org/10.1016/j.apenergy.2020.114530.
[26] Scapino L, Zondag HA, Van Bael J, Diriken J, Rindt CCM. Sorption heat storage for long-term low-temperature applications: A review on the advancements at material and prototype scale. Appl Energy 2017;190:920–48. https://doi.org/10.1016/j.apenergy.2016.12.148.
[27] Stengler J, Bürger I, Linder M. Performance analysis of a gas-solid thermochemical energy storage using numerical and experimental methods. Int J Heat Mass Transf 2021;167:120797. https://doi.org/10.1016/j.ijheatmasstransfer.2020.120797.
[28] Esaki T, Kobayashi N. Study on the cycle characteristics of chemical heat storage with different reactor module types for calcium chloride hydration. Appl Therm Eng 2020;171:114988. https://doi.org/10.1016/j.applthermaleng.2020.114988.

[29] Freni A, Russo F, Vasta S, Tokarev M, Aristov YuI, Restuccia G. An advanced solid sorption chiller using SWS-1L. Appl Therm Eng 2007;27:2200–4. https://doi.org/10.1016/j.applthermaleng.2005.07.023.
[30] Calabrese L, Brancato V, Bonaccorsi L, Frazzica A, Caprì A, Freni A, et al. Development and characterization of silane-zeolite adsorbent coatings for adsorption heat pump applications. Appl Therm Eng 2017;116:364–71. https://doi.org/10.1016/j.applthermaleng.2017.01.112.
[31] Kummer H, Füldner G, Henninger SK. Versatile siloxane based adsorbent coatings for fast water adsorption processes in thermally driven chillers and heat pumps. Appl Therm Eng 2015;85:1–8. https://doi.org/10.1016/j.applthermaleng.2015.03.042.
[32] Bahrehmand S, Khajehpour M, Huttema W, Mccague C, Bahrami M. The effects of graphite flake on specific cooling power of sorption chillers: An experimental study, 2018.
[33] McCague C, Huttema W, Fradin A, Bahrami M. Lab-scale sorption chiller comparison of FAM-Z02 coating and pellets. Appl Therm Eng 2020;173:115219. https://doi.org/10.1016/j.applthermaleng.2020.115219.
[34] He F, Nagano K, Seol S-H, Togawa J. Thermal performance improvement of AHP using corrugated heat exchanger by dip-coating method with mass recovery. Energy 2022;239:122418. https://doi.org/10.1016/j.energy.2021.122418.
[35] Venegas T, Qu M, Nawaz K, Wang L. Critical review and future prospects for desiccant coated heat exchangers: Materials, design, and manufacturing. Renew Sustain Energy Rev 2021;151:111531. https://doi.org/10.1016/j.rser.2021.111531.
[36] Cabeza LF, Solé A, Barreneche C. Review on sorption materials and technologies for heat pumps and thermal energy storage. Renew Energy 2017;110:3–39. https://doi.org/10.1016/j.renene.2016.09.059.
[37] Desai F, Sunku Prasad J, Muthukumar P, Rahman MM. Thermochemical energy storage system for cooling and process heating applications: A review. Energy Convers Manag 2021;229:113617. https://doi.org/10.1016/j.enconman.2020.113617.
[38] van Ravensteijn BGP, Donkers PAJ, Ruliaman RC, Eversdijk J, Fischer HR, Huinink HP, et al. Encapsulation of Salt Hydrates by Polymer Coatings for Low-Temperature Heat Storage Applications. ACS Appl Polym Mater 2021;3:1712–26. https://doi.org/10.1021/acsapm.0c01186.
[39] Goetz V, Elie F, Spinner B. The structure and performance of single effect solid-gas chemical heat pumps. Heat Recovery Syst CHP 1993;13:79–96. https://doi.org/10.1016/0890-4332(93)90027-S.
[40] N'Tsoukpoe KE, Rammelberg HU, Lele AF, Korhammer K, Watts BA, Schmidt T, et al. A review on the use of calcium chloride in applied thermal engineering. Appl Therm Eng 2015;75:513–31. https://doi.org/10.1016/j.applthermaleng.2014.09.047.
[41] Molenda M, Stengler J, Linder M, Wörner A. Reversible hydration behavior of CaCl2 at high H2O partial pressures for thermochemical energy storage. Thermochim Acta 2013;560:76–81. https://doi.org/10.1016/j.tca.2013.03.020.
[42] Yu N, Wang RZ, Lu ZS, Wang LW, Ishugah TF. Evaluation of a three-phase sorption cycle for thermal energy storage. Energy 2014. https://doi.org/10.1016/j.energy.2013.12.044.
[43] Ichinose A, Kobayashi N, Esaki T. Dehydration Reaction and its Acceleration for CaCl2 Hydrate for Chemical Heat Storage. Sci Technol 2020;5:20.

[44] Sögütoglu L-C, Steiger M, Houben J, Biemans D, Fischer HR, Donkers P, et al. Understanding the Hydration Process of Salts: The Impact of a Nucleation Barrier. Cryst Growth Des 2019;19:2279–88. https://doi.org/10.1021/acs.cgd.8b01908.
[45] Obermeier J, Müller K, Arlt W. Thermodynamic analysis of chemical heat pumps. Energy 2015;88:489–96. https://doi.org/10.1016/j.energy.2015.05.076.
[46] Zhang YN, Wang RZ, Zhao YJ, Li TX, Riffat SB, Wajid NM. Development and thermochemical characterizations of vermiculite/SrBr2 composite sorbents for low-temperature heat storage. Energy 2016;115, Part 1:120–8. https://doi.org/10.1016/j.energy.2016.08.108.
[47] Conde MR. Properties of aqueous solutions of lithium and calcium chlorides: formulations for use in air conditioning equipment design. Int J Therm Sci 2004;43:367–82. https://doi.org/10.1016/j.ijthermalsci.2003.09.003.
[48] Ashrae. Ashrae Handbook: Fundamentals. American Society of Heating, Refrigerating and Air-Conditioning Engineers, Incorporated; 2001.
[49] Pátek J, Klomfar J. Solid–liquid phase equilibrium in the systems of LiBr–H2O and LiCl–H2O. Fluid Phase Equilibria 2006;250:138–49. https://doi.org/10.1016/j.fluid.2006.09.005.

Appendixes

Table A1: Correlations of the solid/gas reaction equilibrium of the $CaCl_2/H_2O$ couple: $\ln p_v = \frac{A}{T} + B$.

Equilibrium	A	B	Detail	Reference
1-0	-5573.25	22.07	Fit from an equilibrium curve	[40]
	-8823.67	27.93	Results from thermodynamic calculation	[23]
	-	-	4 experimental points in dehydration 100 mg sample	[43]
	-8632.67	29.92	Fit from an equilibrium curve. Data from [47–49]	[42]
	-6825.96	25.72	Hydration Experimentally obtained with 9700 points Closed THT reactor, controlled cooling rate of -0.1 K/min, ≈80 g sample	Present study
	-8948.64	29.23	Dehydration Experimentally obtained with 5900 points Closed THT reactor, controlled heating rate of 0.1 K/min, ≈80 g sample	Present study
2-1	-5653.12	24.04	Fit from an equilibrium curve	[40]
	-	-	4 experimental points in dehydration 100 mg sample	[43]
	-5927.71	25.05	Fit from an equilibrium curve. Data from [47–49]	[42]
	-6133.27	24.95	Hydration Experimentally obtained with 7300 points Closed THT reactor, controlled cooling rate of -0.1 K/min, ≈80 g sample	Present study
	-7890.06	28.52	Dehydration Experimentally obtained with 7500 points Closed THT reactor, controlled heating rate of 0.1 K/min, ≈80 g sample	Present study
0.3-0	-8335.94	29.45	Hydration Experimentally obtained with 5 points Δs_r^0 and Δh_r^0 fitted from the equilibrium points TGA-DSC, $15\ \mu g$ sample	[41]
2-0.3	-7158.53	27.52	Hydration Experimentally obtained with 5 points Δs_r^0 and Δh_r^0 fitted from the equilibrium points TGA-DSC, $15\ \mu g$ sample	[41]

Table A2: Results for the different experimental campaigns (bulk and deposit)

Implementation	Sample	Average T_m ($T_{H2O}(p_v)$) (°C)*	Average T_H (°C)*	Dehydrated mass of salt (g)	Specific Power of reaction $CaCl_2 \cdot (0\text{-}1)H_2O$ (W/kg of dehydrated salt)	Average temperature lift (1-salt) (K)*	Average temperature lift (2-salts) (K)*	Final advancement	Average driving force**
Salt bed	1	78.6 ±1.6	138.7 ±0.4	47.15 ±0.1	184.1 ±18.5	60.6 ±1.6	40.6 ±1.2	1.93 ±0.02	1.54
	2	82.2 ±1.6	158.6 ±0.3	47.65 ±0.1	44.2 ±4.8	76.8 ±1.6	57.9 ±1.2	0.95 ±0.02	0.96
	3	78.9 ±0.6	148.7 ±0.3	64.2 ±0.1	84.8 ±8.5	70.4 ±0.7	49.9 ±0.5	0.94 ±0.02	1.23
	4	79.1 ±0.6	149 ±0.4	66.45 ±0.1	88.8 ±9.2	70.4 ±0.7	50 ±0.6	0.76 ±0.01	1.23
	5	78.4 ±0.8	149 ±0.4	63.75 ±0.1	77.1 ±7.9	70.9 ±0.9	50.3 ±0.7	0.86 ±0.02	1.21
	6	62.9 ±0.7	138.5 ±0.3	46.6 ±0.1	58.3 ±9.4	75.3 ±0.7	51.4 ±0.6	0.33 ±0.02	0.89
	7	73.7 ±1.6	149.6 ±0.3	53.6 ±0.1	36.3 ±3.8	75 ±1.6	53.7 ±1.2	0.91 ±0.01	1.01
	8	61.5 ±1.2	126.5 ±0.5	53.4 ±0.1	86.7 ±5.4	65 ±1.2	40.6 ±1	1.45 ±0.02	1.31
	9 - Cycle 1	80.3 ±0.6	148.8 ±0.4	/	/	68.3 ±0.7	/	/	1.3
	9 - Cycle 2	80.7 ±0.5	148.9 ±0.4	/	/	67.8 ±0.6	/	/	1.31
Deposit	10	70.4 ±3.6	138.6 ±0.3	20.06 ±0.1	341.1 ±51.4	65.1 ±1.3	43.3 ±0.9	1.33 ±0.04	1.42
	11	72.2 ±2.9	158.9 ±0.3	20.21 ±0.1	130.7 ±34.6	87.1 ±2.9	65 ±2.1	0.37 ±0.04	0.67
	12	81.8 ±1.1	148.9 ±0.3	20.06 ±0.1	345.9 ±52.9	67.2 ±1.3	47.8 ±0.9	1.92 ±0.05	1.33
	13	60.5 ±1.9	130.9 ±2.7	24.21 ±0.1	86.3 ±16.9	71.4 ±4.4	45.8 ±2.8	0.49 ±0.04	1.1
	14	73.9 ±1.3	149 ±0.3	24.51 ±0.1	143.3 ±31.5	75.6 ±1	53.8 ±0.8	0.4 ±0.03	1
	15	60.7 ±0.5	128.4 ±0.2	20.16 ±0.1	92.3 ±15.5	68.5 ±0.6	43 ±0.5	0.79 ±0.04	1.23
	16 - Cycle 1	65.9 ±0.3	138.1 ±0.7	22.35 ±0.1	/	72.6 ±0.4	/	/	1.05
	16 - Cycle 2	66.4 ±0.4	138.4 ±0.3	22.35 ±0.1	/	72.5 ±0.4	/	/	1.06
	16 - Cycle 3	66.2 ±0.6	138.5 ±0.3	22.35 ±0.1	/	72.3 ±0.7	/	/	1.06
	16 - Cycle 4	66 ±2.9	137.1 ±0.3	22.35 ±0.1	/	72.8 ±0.6	/	/	1.05

* The uncertainties correspond to the standard deviation.

** The uncertainty on the equilibrium pressure as function of the temperature is estimated at 10%, this leads an uncertainty on the driving force of 0.11 for all the samples.